Journal of Applied Physics

Broadband downconversion in $Eu^{2+,3+}/Yb^{3+}$ doped calcium aluminosilicate glasses for solar cells applications

Cite as: J. Appl. Phys. **133**, 033102 (2023); https://doi.org/10.1063/5.0131686
Submitted: 23 October 2022 • Accepted: 29 December 2022 • Published Online: 20 January 2023

J. F. M. Santos, R. F. Muniz, E. Savi, et al.

Journal of Applied Physics ARTICLE scitation.org/journal/jap

Broadband downconversion in $Eu^{2+,3+}/Yb^{3+}$ doped calcium aluminosilicate glasses for solar cells applications

Cite as: J. Appl. Phys. **133**, 033102 (2023); doi: 10.1063/5.0131686
Submitted: 23 October 2022 · Accepted: 29 December 2022 ·
Published Online: 20 January 2023

J. F. M. Santos,[1,2,a)] R. F. Muniz,[3] E. Savi,[2] A. A. S. Junior,[2] G. J. Schiavon,[4] A. N. Medina,[2] J. H. Rohling,[2] M. L. Baesso,[2,a)] S. M. Lima,[5] L. H. C. Andrade,[5] T. Catunda,[1] and L. A. O. Nunes[1]

AFFILIATIONS

[1]Instituto de Física de São Carlos, Universidade de São Paulo, Av. Trabalhador São-carlense 400, 13560-970 São Carlos, SP, Brazil
[2]Departamento de Física, Universidade Estadual de Maringá, Av. Colombo 5790, 87020-900 Maringá, PR, Brazil
[3]Departamento de Ciências, Universidade Estadual de Maringá, Av. Reitor Zeferino Vaz, s/n, 87360-900 Goioerê, PR, Brazil
[4]Departamento Acadêmico de Eletrônica, Universidade Tecnológica Federal do Paraná Campus Campo Mourão, Via Rosalina Maria dos Santos 1233, 87301-899 Campo Mourão, PR, Brazil
[5]Grupo de Espectroscopia Óptica e Fototérmica, Universidade Estadual de Mato Grosso do Sul—UEMS, Dourados, MS, Brazil

[a)]**Authors to whom correspondence should be addressed:** jessica.santos@usp.br and mlbaesso@uem.br

ABSTRACT

Novel $Eu^{2+,3+}/Yb^{3+}$ co-doping calcium aluminosilicate glasses prepared under a vacuum atmosphere were developed and characterized from the spectroscopic point of view, as a potential spectral converter for application in solar cells. The emission of near-infrared photons by downconversion due to cooperative energy transfer (ET) from Eu^{2+} and Eu^{3+} to Yb^{3+} in these glasses was reported. Absorption, excitation, emission, and fluorescence decay measurements were performed to examine the ET processes. The occurrence of cooperative energy transfer from Eu^{2+} and/or Eu^{3+} to Yb^{3+} ions was discussed in detail. The obtained samples have high efficiency and broad absorption in the ultraviolet and visible regions. Under 325 nm excitation, the samples achieve intense near-infrared emission, which increases with Yb_2O_3 concentration ($0 < Yb_2O_3 < 1.38$ mol. %). The energy transfer efficiency from $Eu^{2+,3+}$ to Yb^{3+} was evaluated, and a maximum efficiency of ~85% was obtained ($Yb_2O_3 = 1.38$ mol. %).

I. INTRODUCTION

It is well known that the practical efficiency of silicon solar cells is severely limited by the mismatch between solar and silicon absorption spectra.[1–4] In this context, a great challenge is to efficiently convert the energy from the visible region of the solar spectrum, with maximum intensity at 550 nm, to the near-infrared region so that a single junction crystalline silicon solar cell has a major spectral response (1000 nm). Therefore, much effort has been directed to spectral modification by down and upconversion. In this sense, quantum cutting is a particularly attractive process where one incident ultraviolet (UV) photon is transformed into two near-infrared (NIR) photons. There are many reports on the downconversion luminescence processes in rare-earth co-doped systems, such as Re^{3+}–Yb^{3+}, in which Re^{3+} (Tb^{3+}, Tm^{3+}, Eu^{3+} or Pr^{3+}) acts as the absorption centers, respectively.[5–8] For solar cells applications, Yb^{3+} is the best acceptor ion because its emission (~980 nm) matches well the Si bandgap (~1.1 eV). Besides, with a unique energy level structure, Yb^{3+} has only one excited state, minimizing the occurrence of other loss mechanisms. However, the low oscillator strength and narrow bandwidths of 4f–4f absorption transitions limit the practical interest of RE^{3+} sensitizers. This limitation motivated the study of Ce^{3+},[9–11] Eu^{2+},[12–18] and the transition metal Cr^{3+},[19] as a sensitizer for Yb^{3+} due to their intense broadband absorption in the UV/VIS and excellent luminescence properties. Moreover, in many systems, Ce^{3+} and Eu^{2+}, and Cr^{3+} emission match well with the twice energy of the $^2F_{7/2} \rightarrow {}^2F_{5/2}$ transition of Yb^{3+}. Particularly, Eu^{2+} co-doped with Yb^{3+} has been explored in many hosts (crystals, ceramics, and glasses) demonstrating efficient downconversion processes. However,

many papers attribute the observed downconversion effect to a quantum cutting process (where the energy of one donor ion is transferred to two acceptor ions) without supporting experimental evidence, so the underlying physical mechanism is still a subject of debate.[10,11] It should be noticed that in the Eu/Yb system, there is no suitable intermediate level to allow quantum cutting by two sequential resonant ET steps (first-order processes) as observed in the Pr^{3+}/Yb^{3+} system.[2] Therefore, in the case of Eu/Yb, quantum cutting could only be possible by a second-order ET process, which is very unlike compared to the first-order processes.

We have been studying RE-doped glasses in the compositional system $CaO–Al_2O–MgO–SiO^2–RE_2O_3$ ($RE = Eu^{3+}$, Tb^{3+}, Yb^{3+}) which have shown promising characteristics for downconversion and upconversion applications.[5,17,20–23] In silicates, with the addition of intermediates [Al^{3+}] and modifiers [Ca^{2+}] network ions, the glass structure changes due to the formation of non-bridging oxygen (NBO).[24] The presence of modifiers as Na^+, Mg^{2+}, and Ca^{2+} can lead to the softening of the glass network. Consequently, the structure network allows easier incorporation of rare-earth ions, minimizing the formation of clusters, thereby resulting in a better statistical distribution of the dopant ions.[24–26]

Another important aspect of interest in this paper that deserves to be highlighted is the fact that some compositions of calcium aluminosilicate glasses allow the efficient formation of Eu^{2+} ions in their structures when melted under a vacuum atmosphere.[27] Indeed, it is possible to control the ratio of divalent and trivalent Eu ions by simply adjusting the optical basicity of the glass. The increase of non-bridging oxygen concentration in the glass network increases the electron donor power, which decreases the optical basicity and, therefore, reduces the valence state of europium ions. In the present paper, the glass composition was chosen to maximize the fraction of Eu^{2+} in the total europium concentration to about 60%, as shown by magnetization and x-ray absorption near-edge structure (XANES) measurements.[25,27] Similar compositions with high silica content have been shown to improve the integrated visible luminescence of about two orders of magnitude.[27] These experiments demonstrated the possibility of tunable white lighting by combining the effects of matrix composition and pump wavelength.[20] Therefore, these particular characteristics allied to the superior optical, thermomechanical, and resistance against degradation properties,[26,27] suggest calcium aluminosilicates as promising hosts for solar cell applications.

In this paper, $Eu^{2+}–Eu^{3+}–Yb^{3+}$ co-doped calcium aluminosilicate glasses were prepared and the energy transfer (ET) processes from Eu^{2+}/Eu^{3+} to Yb^{3+} were investigated in detail. The spectroscopic characteristics of low and highly doped samples (up to 1.86 mol. % of RE ions) are discussed. A comprehensive study is presented combining the results of absorption, excitation, luminescence, and decay curves measurements. The ET quantum efficiency was estimated from the dependence of the decay time of Eu^{2+} emission with the Yb^{3+} concentration, assuming a first-order process in which, one excited Eu^{2+} generates only one Yb^{3+}, instead of two, as in the case of quantum cutting.[1,2,14] The maximum estimated quantum efficiency of this ET process is ~85%. Several possible energy transfer mechanisms are analyzed considering the effect of Eu^{3+} which has a significant role in all spectroscopic results.

II. MATERIAL AND METHODS

Calcium aluminosilicate glasses (CAS) were prepared with a nominal composition depicted in Table I.

The reagent quantities with purity better than 99.99% were homogeneously mixed in a ball mill for 12h. Afterward, each sample was melted at approximately 1500 °C, using graphite crucibles and under a vacuum atmosphere, for 2h. Thereafter, the quenching was performed, and the annealing was obtained by lowering the sample temperature from about 600 °C to room temperature. Finally, the glasses were cut and polished, presenting excellent optical quality. The samples were cut and polished into a plate shape with dimensions of $2 \times 5 \times 10$ mm. One sample was also prepared with ~200 μm thickness to allow UV absorption measurements in the vicinity of 250 nm.

The absorption spectrum of Eu_2O_3 singly doped CAS glass doped with 2.5 Eu_2O_3 was measured with a UV–vis–near-infrared double beam spectrophotometer (Perkin-Elmer Lambda 900) in the spectral range of 250–1050 nm. The emission spectra was obtained at a front face configuration using a SPEX Fluorolog spectrofluorometer (0.22 m, Spex/1680) equipped with a Xe-lamp as the excitation source. The detection was carried out using a photomultiplier (Hamamatsu/R928) or an InGaAs detector. The same spectrofluorometer was used to excitation spectra with λ_{ob} = 615 and 980 nm. The Eu^{2+} lifetime measurements were obtained using the third harmonic of a Nd:YAG laser at 355 nm (SureliteSLII-10).

III. RESULTS AND DISCUSSION

Figures 1(a)–1(c) show the partial energy level of Eu^{2+}, Eu^{3+}, and Yb^{3+} ions. Several ET processes involving interactions between these ions, such as resonant energy transfer and cooperative excitation transfer can occur in a system co-doped with these ions. The most relevant ET processes are indicated in Figs. 1(a)–1(c). Figure 1(a) depicts a two-step ET process, $Eu^{2+} \rightarrow Eu^{3+} \rightarrow Yb^{3+}$, Fig. 1(b), the direct ET from $Eu^{2+} \rightarrow Yb^{3+}$, and Fig. 1(c), simultaneous ET from one Eu^{2+} to two Yb^{3+} (quantum cutting). These processes will be analyzed based on the spectroscopic data obtained in this paper.

Figure 2(a) presents the UV–vis absorption spectra of Eu_2O_3 single-doped CAS glass (0.45 mol. % of Eu_2O_3). The Eu^{3+} absorption lines are very weak (due to the forbidden nature of f–f transitions on RE^{3+}) and, consequently, are masked by the Eu^{2+} absorption broad bands centered at 250 nm (t_{2g}) and 320 nm (e_g).[27] The Gaussian fit provides FWHM values of 51 and 85 nm to $^8S_{7/2} \rightarrow t_{2g}$ and $^8S_{7/2} \rightarrow e_g$, respectively. These bands are attributed

TABLE I. Samples compositions in mol. %.

Sample	SiO_2	MgO	CaO	Al_2O_3	Eu_2O_3	Yb_2O_3
CAS1	53.19	6.50	28.10	11.75	0.45	0.00
CAS2	53.58	6.55	27.73	11.52	0.46	0.16
CAS3	53.97	6.60	27.35	11.29	0.46	0.33
CAS4	54.77	6.70	26.58	10.81	0.47	0.67
CAS5	55.60	6.80	25.79	10.32	0.47	1.02
CAS6	56.45	6.90	24.98	9.81	0.48	1.38

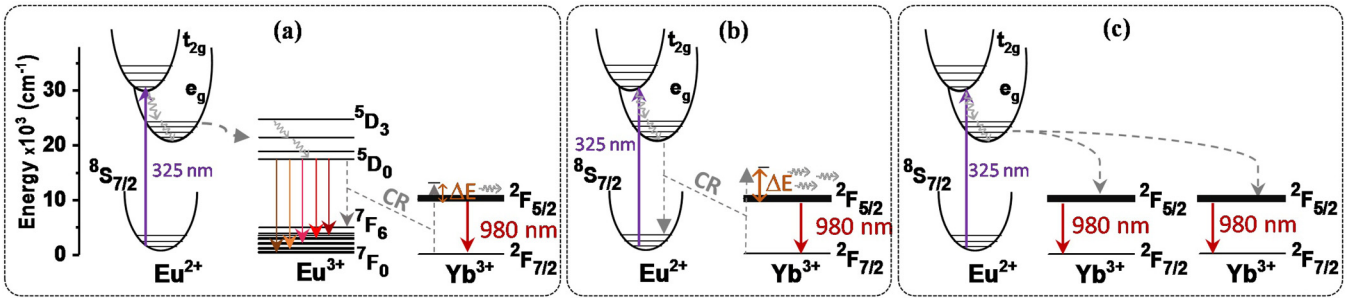

FIG. 1. Partial energy level diagram of $Eu^{2+,3+}$, Yb^{3+} ions, illustrating three possible downconversion ET processes: (a) $Eu^{2+} \rightarrow Eu^{3+} \rightarrow Yb^{3+}$, (b) $Eu^{2+} \rightarrow Yb^{3+}$, and (c) $Eu^{2+} \rightarrow Yb^{3+} + Yb^{3+}$ (quantum cutting).

to the parity-allowed electric dipole transitions, $4f^7(^8S_{7/2}) \rightarrow 4f^65d$ of the Eu^{2+} ions, as observed previously in similar glasses.[27–29] The absorption decreases monotonically in the visible range, but still remains large at ~700 nm ($\alpha \sim 10\ cm^{-1}$), as shown in the inset. In fact, the absorption coefficient tends to zero only above ~900 nm. Figure 2(b) shows the NIR absorption band ranging from ~900 to 1050 nm, characteristic of the $^2F_{5/2} \rightarrow {}^2F_{7/2}$ transition of Yb^{3+}.[30] The inset shows a linear increase of the 980 nm absorption coefficient with Yb_2O_3 concentration, indicating an effective incorporation of Yb^{3+} ions in the glass matrices.

Previous publications on europium-doped aluminosilicate glasses show that the fraction of Eu^{2+}/Eu^{3+} depends on the amount

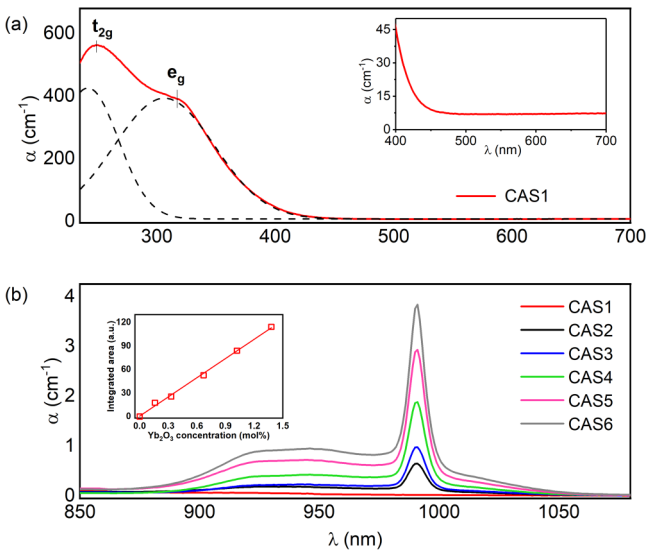

FIG. 2. (a) Absorption spectra in the UV–Vis region of the CAS sample doped with 0.45 mol. % of Er_2O_3 (0.0 Yb_2O_3) fitted by two Gaussian curves (black dashed lines). UV–Vis absorption between 400 and 600 nm is highlighted in the inset. (b) The Yb^{3+} ions absorption is attributed to the $^2F_{5/2} \rightarrow {}^2F_{7/2}$ transition. The Yb_2O_3 concentration varies from 0.0 to 1.38 mol. %. The insets show the Yb concentration dependence.

of silica in the host matrix.[27] X-ray absorption measurements (LIII edge XANES) in samples with several SiO_2 (8.02 mol. % < SiO_2 < 62.31 mol. %) concentrations[27] showed that the ratio $Eu^{2+}/Eu^{2+,3+}$ first increases up to 60% for 53.19 mol. % of SiO_2 (50 wt. % in Fig. 2 of Ref. 27) and then starts to decrease to higher silica concentrations. In this paper, matrices with 53.19–56.45 mol. % of SiO_2 were chosen to maximize the formation of Eu^{2+} ions and, consequently, the glass broadband absorption.

Figures 3(a) and 3(b) present the emission spectra under UV excitation (325 nm) of all samples. Figure 3(a) shows a broad emission band (peaked at ~470 nm) originating from the allowed electronic transition of the excited state 5d to ground state 4f of Eu^{2+} ions ($e_g \rightarrow {}^8S_{7/2}$). Moreover, a narrower weak peak can be noticed at ~615 nm, suggesting the presence of Eu^{3+} most intense emission line ($^5D_0 \rightarrow {}^7F_2$). All visible spectra (400–700 nm) were measured under identical conditions to allow a quantitative comparison of the integrated emissions. The inset indicates a monotonic decrease of Eu^{2+} integrated emission with Yb^{3+} concentration. Figure 3(b) shows the downconversion emission spectrum of Yb^{3+} ($\lambda_{ex} = 325$ nm). A large increase in Yb^{3+} emissions can be observed in the inset due to the efficient downconversion process since Yb^{3+} does not have absorption levels in this region.

The emission spectra under 528 and 457 nm excitation are shown in Figs. 4(a) and 4(b), respectively. These wavelengths were chosen to be in resonance with $^7F_0 \rightarrow {}^5D_1$ and $^7F_0 \rightarrow {}^5D_2$ absorption lines of Eu^{3+}, respectively.[20] Figure 4(a) shows that several narrow peaks (~5 nm) are observed and attributed to the Eu^{3+} transitions from the $^5D_0$ emission level to the indicated states $^7F_0$, $^7F_1$, $^7F_2$, $^7F_3$, and $^7F_4$. The emission spectra of Eu–Yb samples with 457 nm excitation present a strong emission band up to 700 nm and the characteristics of Eu^{3+} emission peaks, as shown in Fig. 4(b). This excitation wavelength is resonant with $^7F_0 \rightarrow {}^5D_2$ Eu^{3+}- absorption transition, but it also excites the Eu^{2+} ions with some efficiency, as can be seen in the insert in Fig. 2 that enlarges the spectra for $\lambda > 400$ nm. In both cases [Figs. 4(a) and 4(b)], the integrated emission decreases with the increase of Yb^{3+} concentration, indicating ET from Eu^{2+} and Eu^{3+} to Yb^{3+} ions, due to downconversion processes. However, this behavior is most remarkable in Fig. 4(b), where the role of Eu^{2+} is greater compared to Fig. 4(a).

The excitation spectra were recorded by monitoring the Eu^{3+} and the Yb^{3+} emissions. Figures 5(a) and 5(b) show the excitation

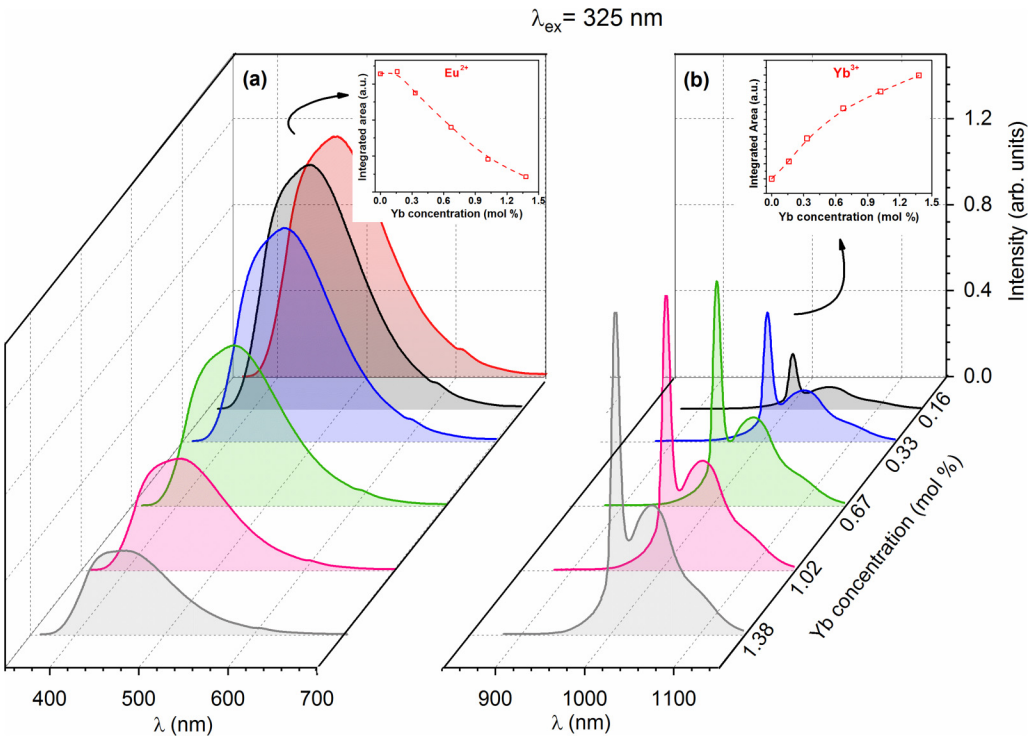

FIG. 3. (a) Visible emission of Eu^{2+} emission spectra, $5d(e_g) \rightarrow {}^8S_{7/2}$, and (b) Yb^{3+} downconversion IR emission spectra, ${}^2F_{5/2} \rightarrow {}^2F_{7/2}$, of CAS glass as a function of Yb_2O_3 concentration. Both spectra were obtained with a 325 nm excitation wavelength. The insets show the respective integrated fluorescence intensity as a function of the Yb^{3+} ion.

spectra monitoring the ${}^5D_0 \rightarrow {}^7F_2$ emission of Eu^{3+} ($\lambda_{ob} = 615$ nm) of the $0.46Eu_2O_3$–$0.16Yb_2O_3$ and $0.48Eu_2O_3$–$1.38Yb_2O_3$, respectively. The nine peaks observed at 315, 359, 378, 391, 410, 461, 530, 575, and 584 nm are attributed to the ground state absorption of Eu^{3+} (${}^7F_0$) to ${}^5H_6$, ${}^5D_4$, ${}^5L_7$, ${}^5L_6$, ${}^5D_3$, ${}^5D_2$, ${}^5D_1$, ${}^5D_0$, and ${}^7F_1 \rightarrow {}^5D_0$, respectively. These narrow peaks are superposed to a "UV tail" and a broader band (~250–500 nm), roughly resembling the absorption spectrum [Fig. 2(a)]. Thus, the excitation spectra could be told apart in two Gaussian broadbands, centered at 250 and 395 nm, in addition to nine narrower Gaussians (typically ~5 nm FWHM). It should be noticed that the broadband [peaked at ~525 nm in Fig. 4(b)] assigned to Eu^{2+} is redshifted concerning the absorption spectra [Fig. 2(a)]. This change in the excitation spectra can be attributed to the extraordinarily strong absorption in the 250–450 nm range. In this spectral range, the absorption coefficient decreases from ~550 to ~10 cm^{-1} [Fig. 2(a)] which is equivalent to the light penetration length varying from ~0.020 to 1 mm, respectively. Reminding that the samples have ~2 mm thickness, the higher Eu^{2+} absorption in the UV [Fig. 2(a)] is compensated by the shorter sample "effective length," modifying the excitation spectra line shape.

The analyses of Figs. 5(a) and 5(b) show that all excitation bands decrease with the increase of Yb_2O_3 content, suggesting that both Eu^{2+} and Eu^{3+} transfer energy to Yb^{3+}. This hypothesis is corroborated by the excitation spectra with $\lambda_{ob} = 980$ nm [Figs. 5(c)–5(d)]. The respective UV–Vis peaks of Eu^{2+} and Eu^{3+} are observed in the same positions presented in Figs. 5(a) and 5(b) and, the Eu^{2+} band's intensities (see blue shaded areas) are greatly increased on elevating the Yb^{3+} doping concentration.

The dependence of the integrated area of the Eu^{2+} broadband (shaded areas in the excitation spectra of Fig. 5) with Yb^{3+} concentration is presented in Fig. 6. The red circles show a decrease in the Eu^{2+} ($\lambda_{ob} = 615$ nm) bands with an increase of Yb^{3+}. The opposite behavior was obtained with $\lambda_{ob} = 980$ nm (blue square). These results allow us to conclude that the increase of Yb^{3+} emission occurs due to the decrease of Eu^{3+} and Eu^{2+} emissions through ET processes.

In a complementary way, the fluorescence kinetics of the broadband emission, attributed to $4f^65d \rightarrow 4f^7$ of the Eu^{2+} [Fig. 3(a)], can give information about the ET processes involved. Figure 7 shows the decay curves monitored at 404 nm, upon pulsed (5 ns) excitation at 355 nm, for samples doped with 0.16 up to 1.38 mol. % of Yb_2O_3. It should be noticed that even the decay curve of the single-doped (Eu_2O_3) sample shows a non-exponential behavior which could be attributed to the ET from Eu^{2+} to neighboring Eu^{3+}. Moreover, this behavior could also be caused by energy migration among Eu^{2+} ions due to a large distribution of Eu^{2+} sites produced by structural disorder, since the 5d levels are strongly sensitive to the ligand field. Nevertheless, a strong decrease of the effective fluorescence lifetime is observed with the increase of Yb_2O_3

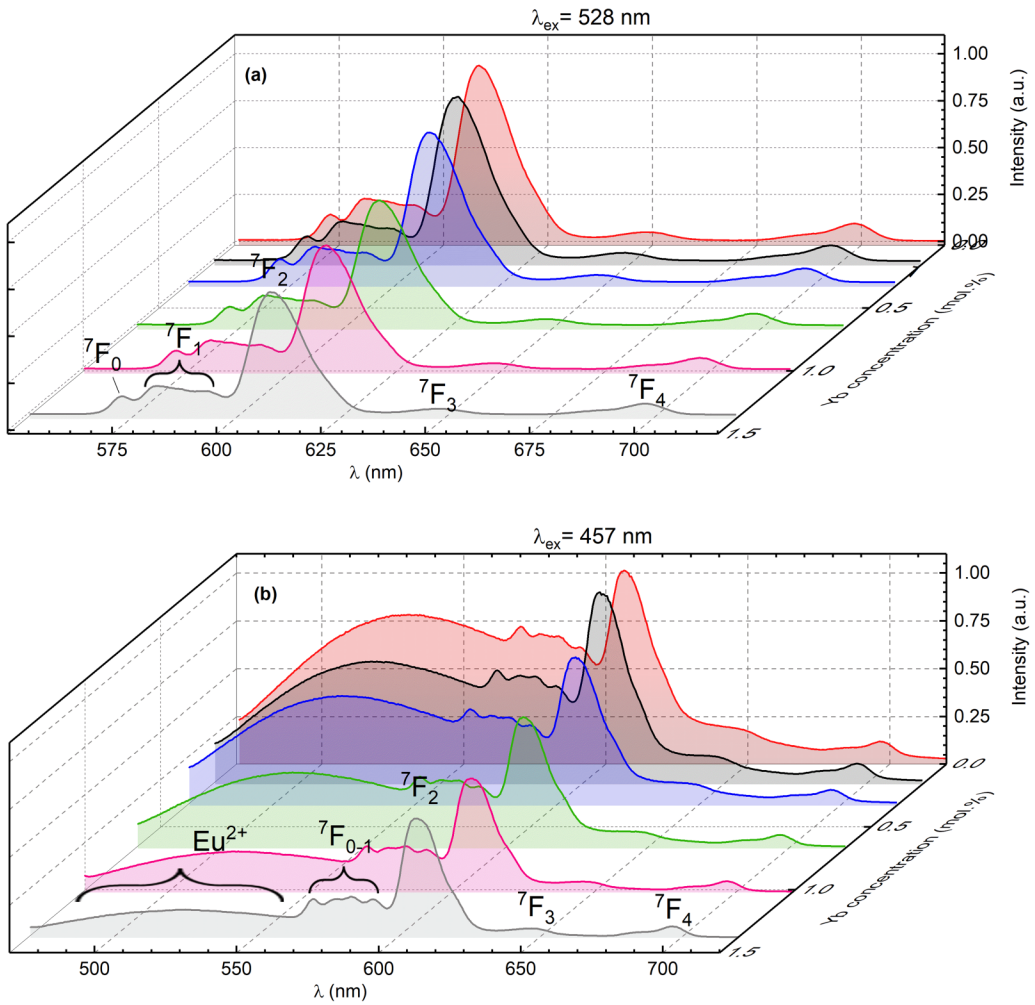

FIG. 4. Emission spectra (a) with λ_{ex} = 528 and (b) λ_{ex} = 457 nm.

concentration in the co-doped samples. This process can be evaluated by the mean decay time as

$$\tau_m = \frac{1}{I(0)} \int_0^\infty I(t)\, dt, \tag{1}$$

in which $I(t)$ is the luminescence intensity and $I(0)$ is the luminescence intensity at t = 0. As the concentration of Yb^{3+} increases from x = 0 to 1.38 mol. %, τ_m drops rapidly from 2.1 to 0.31 μs, as shown in Fig. 8. This behavior can be described by[31]

$$\tau_m(x) = \frac{\tau_m(0)}{1 + (x/C)^p}, \tag{2}$$

in which x (x = 0.0, 0.16, 0.33, 0.67, 1.02, and 1.38). Figure 8 shows that $\tau_m(x)$ is well described by Eq. (2), where the fit results in $\tau_m(0) = 2.05\ \mu$s, $C = 0.67$ mol. %, and p = 1.8. C represents the typical concentration for which $\tau_m(x) = \tau_m(0)/2$, and p ~ 2 are expected for the ET process with dipole–dipole interaction.

From Eq. (2), the ET quantum efficiency (η) can be determined by Eq. (3)[8] assuming that one photon from the Yb^{2+} emission generates one excited Yb^{3+},

$$\eta(x) = 1 - \frac{\tau_m(x)}{\tau_m(0)} = \frac{(x/C)^p}{1 + (x/C)^p}. \tag{3}$$

Figure 8 shows that $\eta(x)$, in blue circles, increases with Yb_2O_3 content reaching a maximum value of ~85% for the glass with 1.38 mol. % of the Yb_2O_3 content. This η value is higher than the typical ones reported in the literature for Eu^{2+}–Yb^{3+} co-doped borate, borosilicate, and calcium aluminosilicate glasses.[14,32,33]

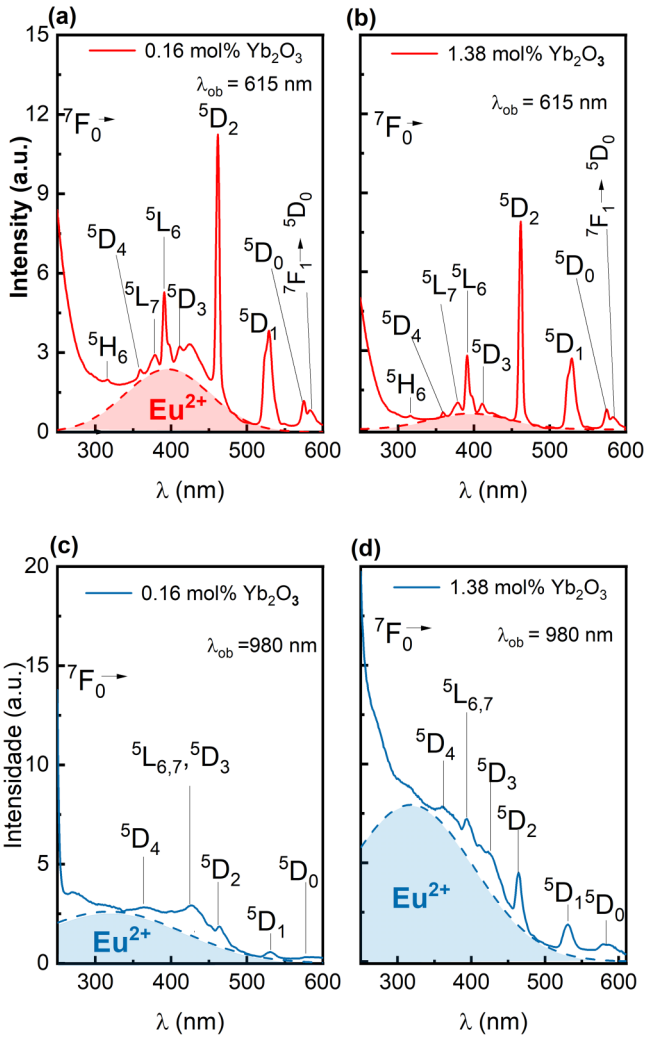

FIG. 5. (a) and (b) The excitation spectra monitoring the 615 nm emission of Eu^{3+} ions doped with 0.16 and 1.38 mol. % of the Yb_2O_3, respectively. Red shaded areas are attributed to the Eu^{2+} absorption bands centered at 250 and 395 nm. (c) and (d) The excitation spectra monitoring the $^2F_{7/2}$–$^7F_{5/2}$ emission (980 nm) of Yb^{3+} ions in CAS glass doped with (c) 0.16 and (d) 1.38 mol. % of the Yb_2O_3. Blue shaded areas represent the $4f(^8S_{7/2}) \rightarrow 5d(e_g, t2_g)$ transitions of the Eu^{2+} ions.

Moreover, the resemblance of Figs. 6 and 8 is remarkable, corroborating the hypothesis of ET from $Eu^{2+}/Eu^{3+} \rightarrow Yb^{3+}$.

The main possible ET mechanisms involving Eu^{2+}, Eu^{3+}, and Yb^{3+} are depicted in Fig. 1. Considering the important role played by Eu^{3+} ions, we think that the most probable route is a two steps ET process, $Eu^{2+} \rightarrow Eu^{3+} \rightarrow Yb^{3+}$. In fact, Figs. 5(a) and 5(b) demonstrate the effective $Eu^{2+} \rightarrow Eu^{3+}$ ET, and Figs. 5(c) and 5(d) show the typical Eu^{3+} absorption peaks in the excitation spectra of Yb^{3+} ($\lambda_{ob} = 980$ nm). The $Eu^{3+} \rightarrow Yb^{3+}$ ET should involves a cross-relaxation process: $^5D_0[Eu^{3+}]$–$^7F_6[Eu^{3+}] \rightsquigarrow {}^2F_{7/2}[Yb^{3+}]$–$^2F_{5/2}[Yb^{3+}]$,

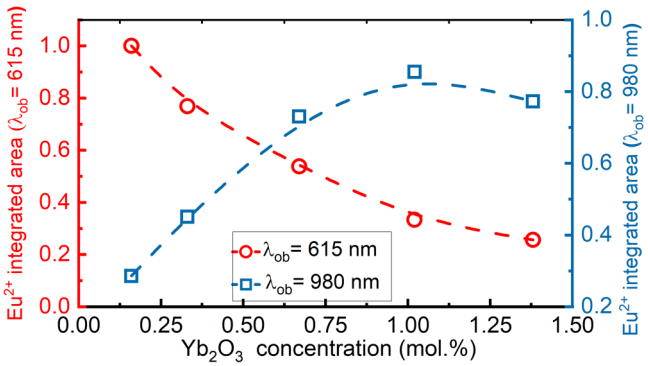

FIG. 6. Variation of integrated area attributed to Eu^{2+} in the excitation spectra (as shown in Fig. 5) as a function of the Yb^{3+} ion concentration. The red circles indicate $\lambda_{ob} = 615$ nm and the blue squares indicate $\lambda_{ob} = 980$ nm.

where the energy released by Eu^{+3} is higher than the one taken by Yb^{3+}. This small energy difference ($\Delta E \sim 1300\ cm^{-1}$) is easily compensated by phonon emission since the phonon energy of CAS glasses is around $1\,100\ cm^{-1}$. Although less likely, other energy transfer processes may also occur. Figure 1(b) depicts direct ET $Eu^{2+} \rightarrow Yb^{3+}$ by CR. In fact, Eu^{2+} emission ($e_g \rightarrow {}^8S_7$) and Yb^{3+} absorption ($\lambda_{ob} = 980$ nm)[28] are extremely broad. The energy of Eu^{2+} is higher than Yb^{3+} by $\Delta E \sim 3500\ cm^{-1}$ so ET can occur assisted by ~3 phonons of the glass matrix. We remind that Eu^{2+} has a very large emission band with a maximum emission wavelength of ~700 nm, as shown in Fig. 4(b). However, we emphasize that this process should be more likely in materials where this energy difference is smaller. For instance, Zhou *et al.*[16] observed a large spectral overlap between the Eu^{2+} emission and the Yb^{3+} absorption bands in a garnet host. Both processes indicated in Figs. 1(a) and 1(b) represent the generation of one Yb^{3+} excitation by one Eu excitation, so quantum efficiency is less than 100% and can be estimated by η in Fig. 8.

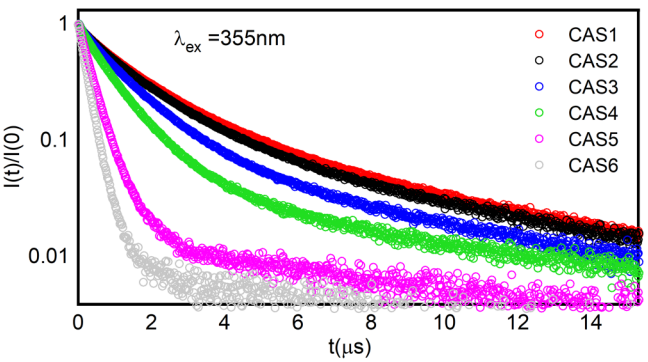

FIG. 7. Luminescence decay curves of Eu^{2+} under pulsed (5 ns) 355 nm excitation for samples with various Yb_2O_3 concentrations. The luminescence signals were detected at 404 nm.

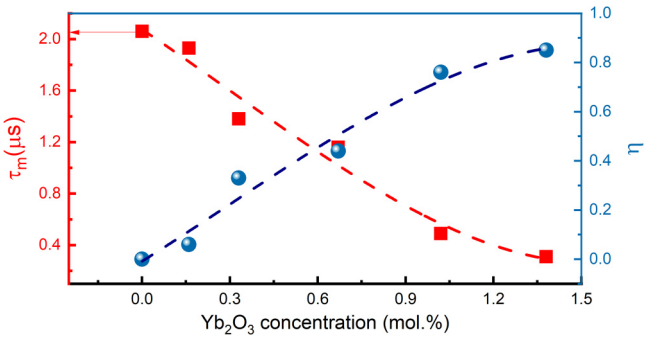

FIG. 8. The variation of average decay time (τ_m) of the 5d (e_g) → 4f($^8S_{7/2}$) Eu^{2+} emission, under excitation at 355 nm (in red) with Yb_2O_3 concentration transition. The blue curve shows the dependence of the ET quantum efficiency, $\eta(x)$, calculated by Eq. (3).

Several papers in the literature[14,15,32,34] have assumed, but not proven,[16] a quantum cutting process that generates two excited Yb^{3+} ions for every Eu excitation, as indicated in Fig. 1(c). This is a second-order cooperative process involving instantaneous energy transfer from one Eu^{2+} to two Yb^{3+} ions, generating two IR photons from one absorbed UV photon. However, Refs. 2 and 35 demonstrated that the second-order ET processes commonly have a probability of 3 orders of magnitude lower than the first-order processes, such as one-step downconversion. Therefore, ET due to quantum cutting should provide a negligible or weak contribution to the Yb^{3+} emission reported in this paper. Finally, other ET processes, like the effect of electron transfer can have a role in the observed downconversion. For instance, electron transfer from $Eu^{2+}+Yb^{3+} \rightarrow Eu^{3+} + Yb^{2+}$ may occur once the presence of Yb^{2+} ions was previously observed in a similar base glass of this paper.[30]

The Vis-to-NIR spectral conversion is reflected in the excitation spectra ($\lambda_{ob} = 980$ nm) of the downconversion materials, therefore, is a desirable broadband excitation for the NIR emission.[8,34] In view of the solar spectrum and practical applications, the more photons absorbed in the range of 250–550 nm, the higher the solar cells' conversion efficiency.[1,7,11,36] In the $Eu^{2+,3+}$–Yb^{3+} doped CAS, Eu^{2+} ions act as broadband spectral sensitizers by absorbing UV–Vis (260–700 nm) photons, which are not efficiently absorbed by silicon solar cells (see the blue curve in Fig. 9).

After energy transfer, the Yb^{3+} acceptors exhibit a strong NIR emission centered at around 1000 nm, which is coupled well with the absorption band of the silicon solar cell. Therefore, $Eu^{2+,3+}$–Yb^{3+} doped CAS glass is comparatively better than the previous downconversion materials doped with a RE^{3+}–Yb^{3+} pair (RE = Nd, Tb, Pr, Tm, and Eu) because the bandwidth of the 4f–5d transition of Eu^{2+} is much broader than that of the 4f–4f transitions of those RE ions.[6,37–40] As shown in Fig. 9, the c-Si solar cells' photoelectric transformation efficiency is the highest near the bandgap (1.1 eV), while the response becomes weak in the high energy region due to thermalization loss. In fact, Fig. 9 shows a broad region 260–700 nm light that can be converted into around 1 μm, where the c-Si response is the highest. As a result, the conversion efficiency of c-Si solar cells can be significantly improved.

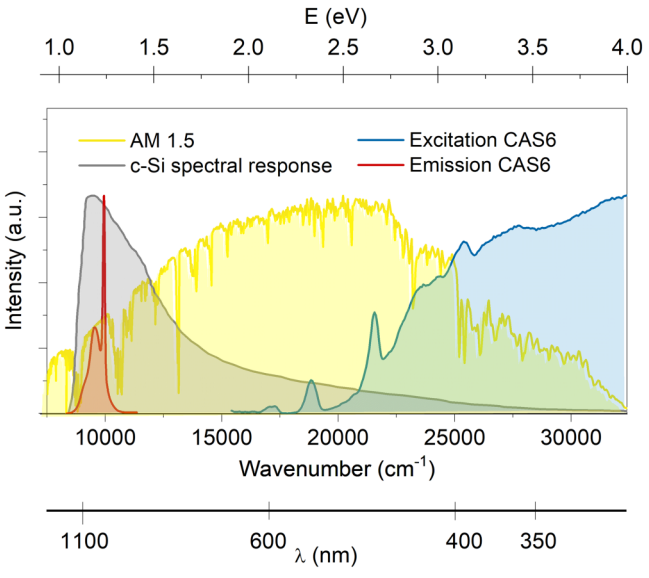

FIG. 9. The yellow background is the solar spectrum (AM1.5G) in the UV–Vis–NIR region. The gray background is the spectral response of c-Si. Blue and red curves are the excitation spectrum (monitored at 980 nm) and NIR emission spectrum ($\lambda_{ex} = 325$ nm) of the 0.48Eu–1.38Yb co-doped glass, respectively.

IV. CONCLUSION

In summary, Eu^{2+}–Eu^{3+}–Yb^{3+} co-doped calcium aluminosilicate glasses were investigated as a downconversion layer candidate to enhance silicon solar cell efficiency. Absorption, excitation, and luminescence spectra show that the luminescence properties are strongly affected by Yb_2O_3 doping concentration. Excitation, emission, and decay measurements indicate the occurrence of energy transfer from Eu^{2+}/Eu^{3+} to Yb^{3+} ions. The ET quantum efficiency (η) was estimated from the decrease of Eu^{2+}(5d) emission decay time with Yb_2O_3. Fixing the Eu concentration (0.45 mol. % of Eu_2O_3), it was observed that η increases monotonically with Yb concentration, reaching η ~ 85% for 1.38 mol. % of Yb_2O_3. The main contribution to the observed data is a two-step process, $Eu^{2+} \rightarrow Eu^{3+} \rightarrow Yb^{3+}$. No evidence of quantum cutting was observed. Anyway, the results show that Eu^{2+} can be a good sensitizer for Yb^{3+} in CAS glasses, providing efficient conversion of the broadband 250–550 nm light excitation to NIR (~980 nm) which can be efficiently absorbed by silicon solar cells.

ACKNOWLEDGMENTS

This work was financially supported by CNPq, CAPES, FINEP, and Companhia Paranaense de Energia Elétrica (COPEL), Projeto P&D 2866-0466/2017-Código ANEEL.

AUTHOR DECLARATIONS

Conflict of Interest

The authors have no conflicts to disclose.

Author Contributions

J. F. M. Santos: Conceptualization (equal); Data curation (equal); Formal analysis (equal); Investigation (equal); Methodology (equal); Validation (equal); Visualization (equal); Writing – original draft (equal); Writing – review & editing (equal). **R. F. Muniz:** Data curation (equal); Formal analysis (equal); Investigation (supporting); Writing – original draft (supporting). **E. Savi:** Investigation (equal); Methodology (equal); Writing – original draft (supporting). **A. A. S. Junior:** Investigation (supporting); Methodology (supporting). **G. J. Schiavon:** Investigation (equal); Methodology (supporting). **A. N. Medina:** Data curation (equal); Formal analysis (equal); Investigation (equal); Methodology (equal); Writing – review & editing (equal). **J. H. Rohling:** Formal analysis (equal); Investigation (equal); Methodology (equal). **M. L. Baesso:** Conceptualization (equal); Data curation (equal); Formal analysis (equal); Funding acquisition (equal); Investigation (equal); Methodology (equal); Project administration (equal); Resources (equal); Supervision (equal); Validation (equal); Visualization (equal); Writing – original draft (equal); Writing – review & editing (equal). **S. M. Lima:** Data curation (equal); Formal analysis (equal); Methodology (equal); Writing – review & editing (equal). **L. H. C. Andrade:** Formal analysis (equal); Investigation (equal); Methodology (equal); Writing – review & editing (equal). **T. Catunda:** Conceptualization (equal); Data curation (lead); Formal analysis (lead); Investigation (equal); Methodology (equal); Supervision (equal); Writing – original draft (equal); Writing – review & editing (equal). **L. A. O. Nunes:** Conceptualization (lead); Data curation (lead); Formal analysis (equal); Investigation (lead); Methodology (lead); Writing – original draft (equal); Writing – review & editing (equal).

DATA AVAILABILITY

The data that support the findings of this study are available from the corresponding authors upon reasonable request.

REFERENCES

[1]Y. Katayama and S. Tanabe, "Downconversion for 1 μm luminescence in lanthanide and Yb^{3+} co-doped phosphors," in *Solar Cells and Light Management: Materials, Strategies, and Sustainability* (Elsevier Ltd., 2019), pp. 415–441.

[2]B. M. Van Der Ende, L. Aarts, and A. Meijerink, "Near-infrared quantum cutting for photovoltaics," Adv. Mater. **21**, 3073 (2009).

[3]E. L. Savi, R. F. Muniz, A. A. J. Silva, G. J. Schiavon, J. W. Berrar, F. R. Estrada, P. Schio, J. C. Cezar, J. H. Rohling, V. S. Zanuto, A. C. Bento, A. N. Medina, L. A. O. Nunes, and M. L. Baesso, "Thin-film of Nd^{3+}–Yb^{3+} co-doped low silica calcium aluminosilicate glass grown by a laser deposition technique," J. Appl. Phys. **131**, 055304 (2022).

[4]A. C. Bento, N. Cella, S. M. Lima, L. A. O. Nunes, L. H. C. Andrade, J. R. Silva, V. S. Zanuto, N. G. C. Astrath, T. Catunda, A. N. Medina, J. H. Rohling, R. F. Muniz, J. W. Berrar, L. C. Malacarne, W. R. Weinand, F. Sato, M. P. Belancon, G. J. Schiavon, J. Shen, L. C. M. Miranda, H. Vargas, and M. L. Baesso, "Photoacoustic and photothermal and the photovoltaic efficiency of solar cells: A tutorial," J. Appl. Phys. **131**, 141101 (2022).

[5]I. A. A. Terra, L. J. Borrero-González, L. A. O. Nunes, M. P. Belanon, J. H. Rohling, M. L. Baesso, and O. L. Malta, "Analysis of energy transfer processes in Yb^{3+}-Tb^{3+} co-doped, low-silica calcium aluminosilicate glasses," J. Appl. Phys. **110**, 083108 (2011).

[6]L. D. A. Florêncio, L. A. Gómez-Malagón, B. C. Lima, A. S. L. Gomes, J. A. M. Garcia, and L. R. P. Kassab, "Efficiency enhancement in solar cells using photon down-conversion in Tb/Yb-doped tellurite glass," Sol. Energy Mater. Sol. Cells **157**, 468 (2016).

[7]G. Lakshminarayana, H. Yang, S. Ye, Y. Liu, and J. Qiu, "Co-operative downconversion luminescence in Tm^{3+}/Yb^{3+}:SiO_2-Al_2O_3-LiF-GdF_3 glasses," J. Phys. D: Appl. Phys. **41**, 175111 (2008).

[8]M. Rai, K. Mishra, S. B. Rai, and P. Morthekai, "Tailoring UV-blue sensitization effect in enhancing near infrared emission in X, Yb^{3+}: $CaGa_2O_4$ (X = 0, Eu^{3+}, Bi^{3+}, Cr^{3+}) phosphor for solar energy conversion," Mater. Res. Bull. **105**, 192 (2018).

[9]J. Ueda and S. Tanabe, "Visible to near infrared conversion in Ce^{3+}-Yb^{3+} Co-doped YAG ceramics," J. Appl. Phys. **106**, 043101 (2009).

[10]A. D. Sontakke, J. Ueda, Y. Katayama, P. Dorenbos, and S. Tanabe, "Experimental insights on the electron transfer and energy transfer processes between Ce^{3+}-Yb^{3+} and Ce^{3+}-Tb^{3+} in borate glass," Appl. Phys. Lett. **106**, 131906 (2015).

[11]L. Zhou, W. Zhou, F. Pan, R. Shi, L. Huang, H. Liang, P. A. Tanner, X. Du, Y. Huang, Y. Tao, and L. Zheng, "Spectral properties and energy transfer of a potential solar energy converter," Chem. Mater. **28**, 2834 (2016).

[12]H. Lin, D. Chen, Y. Yu, Z. Shan, P. Huang, A. Yang, and Y. Wang, "Broadband UV excitable near-infrared downconversion luminescence in Eu^{2+}/Yb^{3+}:CaF_2 nanocrystals embedded glass ceramics," J. Alloys Compd. **509**, 3363 (2011).

[13]J. Sun, W. Zhou, Y. Sun, and J. Zeng, "Broadband near-infrared downconversion luminescence in Eu^{2+}-Yb^{3+} codoped $Ca_9Y(PO_4)_7$," Opt. Commun. **296**, 84 (2013).

[14]J. Zhou, Y. Zhuang, S. Ye, Y. Teng, G. Lin, B. Zhu, J. Xie, and J. Qiu, "Broadband downconversion based infrared quantum cutting by cooperative energy transfer from Eu^{2+} to Yb^{3+} in glasses," Appl. Phys. Lett. **95**, 141101 (2009).

[15]Q. Yan, J. Ren, Y. Tong, and G. Chen, "Near-infrared quantum cutting of Eu^{2+}/Yb^{3+} codoped chalcohalide glasses," J. Am. Ceram. Soc. **96**, 1349 (2013).

[16]L. Zhou, P. A. Tanner, W. Zhou, Y. Ai, L. Ning, M. M. Wu, and H. Liang, "Unique spectral overlap and resonant energy transfer between europium(II) and ytterbium(III) cations: No quantum cutting," Angew. Chem. **129**, 10493 (2017).

[17]V. S. Zanuto, O. A. Capeloto, R. F. Muniz, M. Sandrini, J. H. Rohling, M. L. Baesso, and L. A. O. Nunes, "Two ratiometric thermometry methods based on the interplay between Eu^{2+} and Eu^{3+} and single Eu^{3+} emissions on OH-free low-silica calcium aluminosilicate glass," Mater. Res. Bull. **135**, 111115 (2021).

[18]B. Abbasgholi-NA, O. A. Aldaghri, K. H. Ibnouf, N. Madkhali, and H. Cabrera, "On the absorption and photoluminescence properties of pure ZnSe and Co-doped ZnSe:Eu^{3+}/Yb^{3+} crystals," Appl. Sci. **12**, 4248 (2022).

[19]Z. Wang, L. Zhang, L. Dong, Y. Xu, S. Yin, and H. You, "Luminescent properties and energy transfer of novel NIR $K(Ga/Al)_{11}O_{17}$:Cr^{3+},Yb^{3+} phosphors for solar cells," Mater. Today Energy. **20**, 3 (2021).

[20]S. M. Lima, L. H. D. C. Andrade, J. R. Silva, A. C. Bento, M. L. Baesso, J. A. Sampaio, L. A. D. O. Nunes, Y. Guyot, and G. Boulon, "Broad combined orange-red emissions from Eu^{2+}- and Eu^{3+}-doped low-silica calcium aluminosilicate glass," Opt. Express **20**, 12658 (2012).

[21]J. F. M. dos Santos, N. G. C. Astrath, M. L. Baesso, L. A. O. Nunes, and T. Catunda, "The effect of silica content on the luminescence properties of Tb^{3+}-doped calcium aluminosilicate glasses," J. Lumin. **202**, 363 (2018).

[22]G. S. Bianchi, V. S. Zanuto, F. B. G. Astrath, L. C. Malacarne, I. A. A. Terra, T. Catunda, L. A. O. Nunes, C. Jacinto, L. H. C. Andrade, S. M. Lima, M. L. Baesso, and N. G. C. Astrath, "Resonant excited state absorption and

relaxation mechanisms in Tb^{3+}-doped calcium aluminosilicate glasses: An investigation by thermal mirror spectroscopy," Opt. Lett. **38**, 4667 (2013).
[23]C. Y. Morassuti, S. Finoto, J. R. Silva, L. A. O. Nunes, Y. Guyot, G. Boulon, M. L. Baesso, A. C. Bento, J. H. Rohling, S. M. Lima, and L. H. C. Andrade, "Combination of broad emission bands of $Ti^{3+,4+}/Eu^{2+,3+}$ co-doped OH-free low silica calcium aluminosilicate glasses as emitting phosphors for white lighting devices," J. Alloys Compd. **853**, 155898 (2021).
[24]A. Novatski, A. Steimacher, A. N. Medina, A. C. Bento, M. L. Baesso, L. H. C. Andrade, S. M. Lima, Y. Guyot, and G. Boulon, "Relations among non-bridging oxygen, optical properties, optical basicity, and color center formation in CaO-MgO aluminosilicate glasses," J. Appl. Phys. **104**, 094910 (2008).
[25]J. A. Sampaio, M. C. Filadelpho, A. A. Andrade, J. H. Rohling, A. N. Medina, A. C. Bento, L. M. Da Silva, F. C. G. Gandra, L. A. O. Nunes, and M. L. Baesso, "Study on the observation of Eu^{2+} and Eu^{3+} valence states in low silica calcium aluminosilicate glasses," J. Phys.: Condens. Matter **22**(5), 055601 (2010).
[26]A. Steimacher, N. G. C. Astrath, A. Novatski, F. Pedrochi, A. C. Bento, M. L. Baesso, and A. N. Medina, "Characterization of thermo-optical and mechanical properties of calcium aluminosilicate glasses," J. Non-Cryst. Solids **352**, 3613 (2006).
[27]A. M. Farias, M. Sandrini, J. R. M. Viana, M. L. Baesso, A. C. Bento, J. H. Rohling, Y. Guyot, D. De Ligny, L. A. O. Nunes, F. G. Gandra, J. A. Sampaio, S. M. Lima, L. H. C. Andrade, and A. N. Medina, "Emission tunability and local environment in europium-doped OH-free calcium aluminosilicate glasses for artificial lighting applications," Mater. Chem. Phys. **156**, 214 (2015).
[28]F. M. M. Yasuoka, J. C. Castro, and L. A. O. Nunes, "Optical spectroscopy of Eu^{2+} ions coupled to CN^- and OCN^- molecular ions in KCl," Phys. Rev. B **43**, 9295 (1991).
[29]K. Biswas, A. D. Sontakke, R. Sen, and K. Annapurna, "Luminescence properties of dual valence Eu doped nano-crystalline BaF_2 embedded glass-ceramics and observation of $Eu^{2+} \rightarrow Eu^{3+}$ energy transfer," J. Fluoresc. **22**, 745 (2012).
[30]Y. Guyot, A. Steimacher, M. P. Belançon, A. N. Medina, M. L. Baesso, S. M. Lima, L. H. C. Andrade, A. Brenier, A.-M. Jurdyc, and G. Boulon, "Spectroscopic properties, concentration quenching, and laser investigations of Yb^{3+}-doped calcium aluminosilicate glasses," J. Opt. Soc. Am. B **28**, 2510 (2011).
[31]J. F. M. dos Santos, I. A. A. Terra, N. G. C. Astrath, F. B. Guimarães, M. L. Baesso, L. A. O. Nunes, T. Catunda, and D. Author, "Mechanisms of optical losses in the $^5D_4$ and $^5D_3$ levels in Tb^{3+} doped low silica calcium aluminosilicate glasses," J. Appl. Phys. **117**, 053102 (2015).
[32]Z. Liu, N. Dai, L. Yang, and J. Li, "High-efficient near-infrared quantum cutting based on broadband absorption in Eu^{2+}–Yb^{3+} co-doped glass for photovoltaic applications," Appl. Phys. A **119**, 553 (2015).
[33]Z. Liu, L. Yang, N. Dai, Y. Chu, Q. Chen, and J. Li, "Intense ultra-broadband down-conversion in co-doped oxide glass by multipolar interaction process," Opt. Express **21**, 12635 (2013).
[34]Y. Teng, J. Zhou, S. Ye, and J. Qiu, "Broadband near-infrared quantum cutting in Eu^{2+} and Yb^{3+} ions Co-doped $CaAl_2O_4$ phosphor," J. Electrochem. Soc. **157**, A1073 (2010).
[35]L. van Pieterson, M. F. Reid, R. T. Wegh, S. Soverna, and A. Meijerink, "4fn→4fn-15d transitions of the light lanthanides: Experiment and theory," Phys. Rev. B **65**, 045113 (2002).
[36]H. Lian, Z. Hou, M. Shang, D. Geng, Y. Zhang, and J. Lin, "Rare earth ions doped phosphors for improving efficiencies of solar cells," Energy **57**, 270 (2013).
[37]D. Chemisana, "Building integrated concentrating photovoltaics: A review," Renew. Sustain. Energy Rev. **15**, 603 (2011).
[38]G. Li, C. Zhang, P. Song, P. Zhu, K. Zhu, and J. He, "Luminescence properties in Tb^{3+}/Yb^{3+} codoped phosphate glasses for solar cells," J. Alloys Compd. **662**, 89 (2016).
[39]P. Liu, J. Liu, X. Zheng, H. Luo, X. Li, Z. Yao, X. Yu, X. Shi, B. Hou, and Y. Xia, "An efficient light converter YAB:Cr^{3+}, Yb^{3+}/Nd^{3+} with broadband excitation and strong NIR emission for harvesting c-Si-based solar cells," J. Mater. Chem. C **2**, 5769 (2014).
[40]Q. Y. Zhang, G. F. Yang, and Z. H. Jiang, "Cooperative downconversion in $GdAl_3(BO_3)_4$: RE^{3+}, Yb^{3+} (RE = Pr, Tb, and Tm)," Appl. Phys. Lett. **91**, 051903 (2007).